RSC Advances

PAPER

View Article Online
View Journal | View Issue

Cite this: *RSC Adv.*, 2024, **14**, 1549

Poly(3,4-ethylenedioxythiophene):polystyrene sulfonate (PEDOT:PSS) as an insulin carrier in silk fibroin hydrogels for transdermal delivery *via* iontophoresis†

Phimchanok Sakunpongpitiporn,[a] Rawita Morarad,[a] Witthawat Naeowong,[b] Sumonman Niamlang[c] and Anuvat Sirivat *[a]

In this study, silk fibroin (SF) was utilized as the starting material to fabricate physically crosslinked hydrogels. Poly(3,4-ethylenedioxythiophene):polystyrene sulfonate (PEDOT:PSS) was synthesized and characterized as a drug carrier, with insulin as the model drug. PEDOT:PSS, with a high electrical conductivity of 1666 ± 49 S cm^{-1}, interacted with insulin molecules *via* electrostatic interaction by replacing the dopant PSS molecules. Insulin-loaded PEDOT:PSS embedded in the SF hydrogel resulted in an increase in the degree of swelling, pore size, and mesh size of the hydrogel. In the *in vitro* release and release-permeation experiments, the amounts of insulin release and release-permeation were investigated using a modified Franz diffusion cell, under the effects of SF concentrations, electric fields, and pH values. The amounts of insulin release and release-permeation from the pristine SF hydrogel and the PEDOT:PSS/SF hydrogel followed the power laws with the scaling exponents close to 0.5, indicating the Fickian diffusion or the concentration gradient. Under electric fields, with or without PEDOT:PSS used as the drug carrier, the insulin amount and diffusion coefficient were shown to increase with the increasing electric field due to the electro-repulsive forces between the cathode and insulin molecules and SF chains, electroosmosis, and SF matrix swelling. The SF hydrogel and PEDOT:PSS as the drug carrier are demonstrated herein as new components in the transdermal delivery system for the iontophoretically controlled insulin basal release applicable to diabetes patients.

Received 9th October 2023
Accepted 16th December 2023

DOI: 10.1039/d3ra06857a

rsc.li/rsc-advances

1. Introduction

Diabetes mellitus is a metabolic disease as identified with hyperglycaemia, glycosuria, and hyperlipidemia; they are caused by either low insulin secretion by cells or low insulin binding efficiency, resulting in high blood glucose levels.[1–3] Diabetes mellitus can be classified into type 1 diabetes mellitus (T1DM), type 2 diabetes mellitus (T2DM), gestational diabetes, and special types of diabetes.[4] T1DM is known as the autoimmune diabetes as characterized by the absolute insulin deficiency due to the damaged pancreatic beta-cell function. T2DM is known as the insulin resistance and secretion as the body uses insulin inefficiently or is not able to produce insulin sufficiently.[3] The treatment of diabetes requires a constant monitoring of blood glucose levels along with the required insulin administration. Diabetes patients typically inject insulin three times daily before each meal (prandial insulin) and one time at bedtime (basal insulin).[5] However, insulin is a peptide hormone that can be destroyed by a gastric acid if taken orally.[6] Therefore, there have been various alternative medical devices, such as syringes, pumps, jet injectors, pens, transdermal patches, and nasal sprays, developed to administer insulin.[2]

The drug delivery system (DDS) is a system that delivers a drug to the body site and maintains the desired drug concentration throughout the dose duration.[7,8] In general, the systemic routes of the drug administration can be classified into 2 types, namely, the enteral and parenteral routes. The enteral route includes oral and rectal administration. The parenteral route includes injection, inhalation, and transdermal administration. A continuous delivery method is the transdermal drug delivery system (TDDS) using a transdermal patch, as first developed in the 1970s and approved by FDA in 1978.[9]

A transdermal patch is placed onto the skin to deliver the specified drug dose into the bloodstream.[10] The advantage of the TDDS is the stable and constant drug level in the blood

[a]*The Conductive and Electroactive Polymers Research Unit, The Petroleum and Petrochemical College, Chulalongkorn University, Bangkok, 10330, Thailand. E-mail: anuvat.s@chula.ac.th*

[b]*Division of Perioperative and Ambulatory Medicine, Department of Medicine, Faculty of Medicine, Chulalongkorn University, Bangkok, 10330, Thailand*

[c]*Department of Materials and Metallurgical Engineering, Faculty of Engineering, Rajamangala University of Technology Thanyaburi, Pathumthani, 12110, Thailand*

† Electronic supplementary information (ESI) available. See DOI: https://doi.org/10.1039/d3ra06857a

stream, and the avoidance of the first pass metabolism as the gastrointestinal tract is not involved.[11] The human skin consists of 3 layers, namely, the epidermis, dermis, and hypodermis. The epidermis is the outer layer of the skin which comprises stratum corneum (SC). The stratum corneum (SC) acts as the barrier that allows only lipophilic drug with a molecular weight less than 500 g mol^{-1} to permeate.[12] Various techniques have been developed to overcome the skin permeation resistance. There are generally two TDDS methods, namely, the active (external stimuli) and passive methods.[11] The passive method involves modifying the drug with chemical enhancers such as liposomes to enhance diffusion or permeability into the skin. However, the delivered drug amount *via* the passive method is still limited by the skin resistance.[13] The active method involves the use of external stimuli such as iontophoresis, magnetophoresis, microneedles, laser radiation, and ultrasound, which act as the driving forces to deliver the drug into the skin.[14] An attractive and simple method is the iontophoresis. The iontophoresis technique involves the use of an electric field with a low voltage and electric current (less than 0.5 mA cm^{-2}) to repel or push the drug through the skin.[11,15]

Most matrices to accommodate drugs are made of polymers, as they are non-toxic and can provide a constant drug delivery rate to the body. The typical polymers employed as drug matrices are hydroxypropyl methyl ether (HPMC), silicone rubber, polypropylene and ethylene vinyl acetate (EVA) copolymers, ethyl acrylate and methyl methacrylate copolymers, and polyethylene glycol (PEG).[16] A physical form of the polymer that has been utilized as the drug reservoir or matrix in TDDS is hydrogel. A hydrogel consists of a three-dimensional network structure that can absorb and retain water in the porous structure.[17] Typical polymers used for hydrogels are carboxymethyl chitosan, polyvinyl alcohol hydrogels, carrageenan, alginate, and agarose amongst many others. The hydrogels can be classified into 2 types: the physically crosslinked network (transient junction) and the chemically crosslinked network (permanent junction).[18] The physical crosslink is deemed more suitable than the chemical crosslink in terms of non-toxicity, higher water absorption, and reversible network interaction. Several interactions can be involved in the physically crosslinked hydrogels: hydrogen bonding; ionic force; and hydrophobic force.[19]

Silk fibroin (SF) from *Bombyx mori* can form a physically crosslinked hydrogel *via* chain entanglement and hydrogen bonding between adjacent chains.[20] The properties of SF are biocompatibility, biodegradability, and mechanical stability. SF uses are common in biomedical and cosmetic applications such as drug delivery, wound healing, injectable scaffolds, gene therapy, and soft tissue regeneration.[21] Generally, the silk fibroin (SF) hydrogels can be fabricated under various influences such as temperature, shear force, ultrasound, pH, electric fields, surfactants, photo crosslinking, irradiation, and chemical agents.[22] Each technique affects various gelation properties such as the mesh size.[23] In this work, the temperature mode was carried out to fabricate SF hydrogels, as it allowed physical crosslinking. The physical crosslink shows non-toxicity and high biocompatibility, which are the required properties in the transdermal drug release.[22]

The drug release from a hydrogel as the drug matrix in the iontophoresis mode can be further improved *via* the use of a drug complex carrier. Conductive polymers (CPs) are promising candidates for use as drug carriers; they are responsive to electrical stimuli *via* releasing the drug, and in addition, they improve the overall matrix electrical conductivity.[24] Poly(3,4-ethylenedioxythiophene):polystyrene sulfonate (PEDOT:PSS) is an attractive CP, as it possesses high electrochemical stability, high electrical conductivity, low energy band gap, high biocompatibility, solubility in water, and the ease to fabricate the hydrogel itself.[25] PEDOT:PSS-based hydrogels have been utilized in various applications: as electrodes in biofuel cells and biosensors; and as matrices in drug release.[26,27] In this work, PEDOT:PSS was chosen and utilized as the drug carrier embedded in the SF hydrogel.

There have been several works along the approach of using biobased hydrogels as drug matrices and iontophoresis coupled with CPs as drug carriers. Jin *et al.* studied metformin release where chitosan was used as the matrix. The amount of metformin release was 96.87% at 30 h.[28] Mahmood *et al.* studied the diloxanide furoate release by using pectin-*co*-polyacrylic acid (MAA) hydrogels. The amounts of diloxanide furoate release at pH values of 1.2 and 7.4 were 8.50% and 75.12%, respectively.[29] Ha *et al.* studied doxorubicin (DOX) release under various electrical voltages. Alginate mixed with gelatin methacrylate (GelMA) and silver nanowires (AgNWs) was used as the matrix and the conductive material, respectively. The amounts of DOX release were 11% and 60% at $E = 0$ and $E = 3$ V in 6 h, respectively.[30] Cai *et al.* investigated the insulin release where polyvinyl alcohol (PVA) and glycerol were utilized as the matrix and the physical crosslinker, respectively. The amount of insulin release was 49.7% in 60 h. In the *in vivo* experiment, a rat was used, in which the blood glucose decreased by more than 50% within 6 days.[31] Saramas *et al.* investigated the metformin release by using κ-Carrageenan (κC) as the matrix. The amounts of metformin release at 0, 3, and 6 V were 92.97%, 95.47%, and 96.72%, whereas the times to equilibrium were 7, 4.5, and 2 h, respectively.[32] Mongkolkitikul *et al.* studied the ibuprofen release where pectin and poly(3-methoxydiphenylamine) (P3DPA) were used as the hydrogel matrix and the conductive polymer, respectively.[33] Paradee *et al.* studied the diclofenac release where dextran and poly(2-ethylaniline) (PEAn) were used as the matrix hydrogel and the conductive polymer, respectively.[34]

In this work, insulin, SF, and PEDOT:PSS were used as the model drug, matrix, and CP drug carrier, respectively. The objectives of this study are to fabricate and systematically characterize insulin-loaded PEDOT:PSS/SF hydrogels; to investigate the insulin release behavior from the pristine SF and PEDOT:PSS/SF hydrogels under the effects of SF concentrations and electric fields; to investigate the insulin release-permeation behavior from the PEDOT:PSS/SF hydrogels under the effects of electric fields and pH values. It will be shown here that PEDOT:PSS as the drug carrier and the present PEDOT:PSS/SF hydrogels are potential as the transdermal drug system to deliver basal insulin under iontophoresis with the controllable drug release rate, amount, and duration.

2. Materials and methods

2.1 Materials

Silk cocoon (*Bombyx mori*, 99.0% purity, grade B (diameters between 1.8 and 2.0 cm), Chul Thai Silk) was used as the starting matrix material. Sodium carbonate ($Na_2CO_3 \geq 99.8\%$ purity, AR grade, Riedel-de Haen) was used to extract sericin from the silk cocoon. Calcium chloride ($CaCl_2$, 99.0% purity, AR grade, Ajax Finechem), ethanol (C_2H_5OH, 99.0% purity, AR grade, Burdick & Jackson), and de-ionized water were used for dissolving the degummed silk cocoon. Snakeskin dialysis tubing (Thermo Scientific, MWCO 3500) was used in the dialysis process. 3,4-Ethylenedioxythiophene (EDOT, 97% purity, Sigma-Aldrich) and poly(styrenesulfonate) (PSS, Mw of 75 000 g mol^{-1}, 99% purity, Sigma-Aldrich) were used for synthesizing PEDOT:PSS, while sodium persulfate ($Na_2S_2O_8$, 98% purity, Sigma-Aldrich) was used as the oxidant. Methanol (CH_3OH > 99.8% purity, RCI Labscan) and acetone (C_3H_6O, 99.5% purity, RCI Labscan) were used as the washing solvent and for collecting the PEDOT:PSS precipitate. De-ionized water was used as the solvent in the synthesis of PEDOT:PSS. Human insulin (recombinant, expressed in yeast, Sigma-Aldrich) was used as the model drug. Sodium hydrogen carbonate ($NaHCO_3$, ACS grade, Merck) was used as the solvent for dissolving insulin. Sodium phosphate monobasic dihydrate ($NaH_2PO_4 \cdot 2H_2O$, 99.0% purity, Sigma-Aldrich) and sodium phosphate dibasic dihydrate ($Na_2H_2PO_4 \cdot 2H_2O$, 99.0% purity, Sigma-Aldrich) were used for the preparation of phosphate buffer solutions (PBS, pH values of 5.5 and 7.4).

2.2 Synthesis of poly(3,4-ethylenedioxythiophene):polystyrene sulfonate (PEDOT:PSS)

PEDOT:PSS was synthesized following the procedure previously reported by Sakunpongpitiporn *et al.*, 2019.[35] First, 5.0 g (4.95 ml) PSS was slowly dropped into de-ionized water (100 ml) and continuously stirred for 1 hour. Next, 0.5 g (0.38 ml) of EDOT at an EDOT : PSS weight ratio of 1/11 was slowly added into the solution which was continuously stirred for 1 hour. After that, 1.67 g $Na_2S_2O_8$ at an EDOT : $Na_2S_2O_8$ mole ratio of 1 : 2 was added into the solution and continuously stirred at room temperature (27 ± 1 °C) for 24 hours. The color of the solution changed from clear to dark blue.[36] Finally, the PEDOT:PSS precipitate was washed with a mixed solution of C_3H_6O (30 ml) and CH_3OH (200 ml) and centrifuged at 9000 rpm. After that, it was dried in an oven at 70 °C for 10 h.

2.3 Preparation of insulin-loaded PEDOT:PSS

First, 0.15 g PEDOT:PSS powder was dissolved in DI-water and stirred at 60 °C for 72 hours to obtain a 3% w/v PEDOT:PSS solution. Then, 7.0 mg of insulin was dissolved in 0.125 mM (0.11 g) $NaHCO_3$ solution and stirred at room temperature for 1 hour.[37] The insulin solution was added into the PEDOT:PSS solution and stirred at room temperature for 48 hours.

2.4 Preparation of the SF solution

The SF solution was prepared following the procedure previously reported by Sakunpongpitiporn *et al.*, 2022.[38,39] First, 2.0 g of silk cocoon was added into 0.5 g Na_2CO_3 solution (100 ml) at 100 °C for 30 min to remove sericin. The silk fibroin precipitate was rinsed with 250 ml DI-water. The degumming process was repeated three times.[40] After that, the degummed silk was dried at room temperature for 2 weeks to obtain the silk fiber. Then, 15 g degummed silk fiber was slowly added (1 g at a time) and dissolved in a ternary solvent consisting of $CaCl_2 : H_2O : C_2H_5OH$ at a mole ratio of 1 : 8 : 2 (73.5 g : 36 g : 18 g) at 70 °C for 4 hours.[41] The solution was dialyzed in DI-water using a snakeskin dialysis tubing for 72 hours. The solution was centrifuged at 8000 rpm to remove the remaining impurities and to obtain the SF solution. The SF solution was kept in a refrigerator at 7 °C.

2.5 Preparation of insulin-loaded PEDOT:PSS/SF hydrogels

The SF solution was stirred at room temperature for 30 min. Next, the SF solution was diluted to various concentrations (3.0, 4.0, and 5.0% w/v of the final mixture), each with a total volume of 20 ml. The SF solution was slowly stirred at 60 °C for 1 hour. After that, the insulin-loaded PEDOT:PSS solution (15 ml) was added into the SF solution (20 ml) to make a final mixture of 35 ml under stirring at room temperature for 30 min. Finally, the mixture solution was poured onto a Petri dish (7.0 cm) and left at 40 °C for 6 hours to obtain a hydrogel in a semi-dry state prior to use. The insulin-loaded PEDOT:PSS/SF hydrogels were then cut into pieces of 0.15 ± 0.03 mm thickness and 1.0 cm radius.

2.6 Preparation of phosphate buffer saline (PBS buffer)

PBS buffer solutions (0.1 M, pH 7.4, and 0.067 M, pH 5.5) were prepared by dissolving 1.17 g of $NaH_2PO_4 \cdot 2H_2O$ and 7.57 g $Na_2H_2PO_4 \cdot 2H_2O$ into 500 ml of DI-water for the PBS pH of 7.4, and by dissolving 4.56 g of $NaH_2PO_4 \cdot 2H_2O$ and 12.00 g of $Na_2H_2PO_4 \cdot 2H_2O$ into 500 ml of distilled water for the PBS pH of 5.5. The PBS solutions were stirred continuously at room temperature for 1 hour to obtain homogeneous solutions. The PBS buffers were used as the medium in the receptor part of the modified-Franz diffusion cell.

2.7 Characterizations

2.7.1 pH. The pH values of the PEDOT:PSS, insulin, insulin-loaded PEDOT:PSS, and PBS buffer solutions were measured using a pH meter (OHAUS, Starter 300). It was operated at room temperature and DI-water was used for rinsing.

2.7.2 Fourier transform infrared (FT-IR) spectroscopy. The functional groups and interactions of the insulin-loaded PEDOT:PSS, insulin-loaded PEDOT:PSS/SF hydrogels and insulin-loaded SF hydrogels were identified using a Fourier transform infrared spectrometer (Nicolet, iS 5, ID7). The spectrometer was operated in the absorbance mode, in the wavenumber range of 650–4000 cm^{-1}, with 64 scans and a resolution of 4 cm^{-1} at room temperature. In the sample preparation, the PEDOT:PSS and insulin-loaded PEDOT:PSS powders were mixed with a KBr powder using a hydraulic machine at a pressure of 300 psi for 30 s.

2.7.3 Simultaneous thermal analyzer (STA). The thermal behaviors of the PEDOT:PSS, insulin, insulin-loaded PEDOT:PSS, insulin-loaded PEDOT:PSS/SF hydrogels, and insulin-loaded SF hydrogels were determined using a simultaneous thermal analyzer (STA; Netzsch, STA 449F3). The STA instrument was operated between 30 and 800 °C at a heating rate of 10 °C min^{-1} in a nitrogen atmosphere. Each sample was weighted between 4 and 10 mg and placed in a platinum pan. Prior to the tests, all samples were dried in an oven at 70 °C for 12 h.

2.7.4 X-ray photoelectron spectroscopy (XPS). The element analysis of PEDOT:PSS and insulin-loaded PEDOT:PSS was performed using a X-ray photoelectron spectrometer (Kratos, Axis Ultra DLD). The XPS instrument was operated with a monochromatic Al-Kα radiation source at 160 eV for a survey scan of 40 eV for the narrow scan. The XPS spectra were recorded using the C 1s spectra as the reference (binding energy 284.8 eV). Each sample was placed on a sample holder with the carbon tape, and then the copper grid was used as the reference.

2.7.5 Scanning electron microscopy (SEM). The morphology of PEDOT:PSS, insulin, insulin-loaded PEDOT:PSS, SF and PEDOT:PSS/SF hydrogels was investigated using a scanning electron microscope (Hitachi, S-4800). The instrument was operated at 2 kV and 10 μA current. The SF and PEDOT:PSS/SF hydrogels were first soaked in a PBS buffer (pH 7.4) until the swollen samples reached equilibrium. After that, they were frozen in a refrigerator (Meling Biomedical, YCD-EL-300) at −20 °C for 7 days. Next, they were lyophilized in a freeze-drier (Biobase, BK-FD 10) at −40 °C for 16 hours. They were rapidly frozen with liquid nitrogen (−40 °C). PEDOT:PSS, insulin, and insulin-loaded PEDOT:PSS were dried in an oven at 70 °C for 12 hours. Each sample was placed on a holder with a carbon adhesive tape and coated with a platinum layer.

2.7.6 Surface area analyzer (BET). The mesh sizes of the SF and PEDOT:PSS/SF hydrogels of various concentrations were measured using a surface area analyzer (BET; Quantrachome, Autosorb IQC). All samples were immersed in a PBS buffer until the samples reached the swollen state. After that, they were frozen in a refrigerator (Meling Biomedical, YCD-EL-300) at −20 °C for 7 days. Next, they were lyophilized in a freeze-drier (Biobase, BK-FD 10) at −40 °C for 16 hours. They were rapidly frozen with liquid nitrogen (−40 °C). Then, 0.2–0.3 g of samples were outgassed at 50 °C for 24 h before the absorption measurement in a helium atmosphere. The mesh sizes were determined in a nitrogen atmosphere.

2.7.7 Swelling test. The SF and PEDOT:PSS/SF hydrogels (a circular disk shape of radius 1.0 cm and thickness 0.15 mm) were immersed in 0.1 M PBS buffer (15 ml, pH values 5.5, 7.4) without and with electric voltages (E) of 3.0 and 6.0 V. The electric voltages were directly applied on each sample with the cathode electrode connected to a power supply (Tektronix, PS 280). The anode electrode was immersed in a PBS buffer. Each sample was placed on a piece of filter paper and weighed at various times with 5–20 min intervals. The degree of swelling (%) of the SF hydrogels was calculated using eqn (1):[42]

$$(\%)\text{degree of swelling} = \frac{W_s - W_d}{W_d} \times 100 \quad (1)$$

where W_d is the weight of the sample after drying at 27 °C (g) and W_s is the weight of the swollen sample (g).

2.7.8 Cytotoxicity. The cytotoxicity of SF and PEDOT:PSS/SF hydrogels was determined *via* an MTT cytotoxicity assay (ISO 10993-5: 2009) using human skin fibroblast cells. A cell suspension containing 1×10^5 cells per ml CRL-2522 in a complete DMEM was added into a 96-well plate. It was incubated at 37 ± 1 °C, 5 ± 0.1% CO_2 and 95 ± 5 relative humidity for 24 ± 2 h to obtain confluent monolayers of cells prior to testing.

2.7.9 UV-visible spectrometer. The characteristic peaks and the amounts of insulin release and release-permeation at various times were determined using a UV-visible spectrometer (TECAN, Infinite M200). The absorbance spectra of insulin were recorded between the wavelengths of 230 and 1000 nm, where the absorbance peak was located at 274 nm.[43] The measured absorbance intensities were converted to insulin concentrations by the calibration curves (pHs = 5.5 and 7.4).

2.7.10 Actual amounts of drug loaded. The loaded amounts of insulin in the insulin-loaded SF and insulin-loaded PEDOT:PSS/SF hydrogels were determined by dissolving each sample (radius = 1.0 cm, thickness = 0.15 mm) in 125 mM $NaHCO_3$ (0.11 g $NaHCO_3$ in 10 ml H_2O). Next, 0.1 ml of the solution was added into 3 ml of the PBS buffer (pH 7.4) and stirred at 100 rpm for 2 hours. The amounts of insulin in the solution were determined using a UV-visible spectrometer at a wavelength of 274 nm.[43]

2.7.11 *In vitro* drug release study. The drug release of the insulin-loaded SF and insulin-loaded PEDOT:PSS/SF films was investigated using the modified Franz diffusion cells kept at 37 ± 0.5 °C with circulating water. The modified Franz diffusion cells comprised two parts: the receptor and the donor. The receptor part contained the PBS buffer (pH 7.4, 15 ml), which was continuously stirred at 150 rpm during the release experiment period (36 hours). The donor part consisted of the insulin-loaded SF or insulin loaded PEDOT:PSS/SF hydrogel. Each sample was placed on the top of a nylon net in the receptor part. Different voltages (0, 3, and 6 V) were applied to the samples by the cathode connected to a power supply (Tektronix, PS 280) attached on top of the sample. The resulting currents and intensities were measured to be 2.31–4.13 μA and 7.36×10^{-4}–1.32×10^{-3} mA cm^{-2}, respectively. In the experiments, the SF and PEDOT:PSS/SF hydrogels initially absorbed the PBS buffer (pH 7.4) from the receptor part to become fully hydrated to allow the insulin or insulin-loaded PEDOT:PSS to diffuse into the receptor part. A PBS buffer sample (0.1 ml) was taken out from the receptor part at different times and replaced with an equal volume of the fresh PBS buffer (pH 7.4).

2.7.12 *In vitro* drug release-permeation study. The drug release-permeation of the insulin-loaded SF and insulin-loaded PEDOT:PSS/SF hydrogels was investigated using the pig belly skin as the membrane instead of the nylon net in the donor part. The hairs on the pig belly skin and subcutaneous fat were first removed. The pig belly skin was cut into a circular disk shape (diameter of 2.0 cm and thickness of 0.2 cm). Next, the pig belly skins were immersed in the PBS buffer (pHs 7.4 or 5.5) for 16 hours, and kept in a refrigerator at 7 °C, prior to use. The

resulting currents and intensities were measured to be 2.21–3.12 μA and 7.04×10^{-4}–9.94×10^{-4} mA cm^{-2}, respectively.

2.7.13 Release characteristics of insulin from insulin-loaded SF and insulin-loaded PEDOT:PSS/SF hydrogels. The power law model can be used to classify the drug release and release-permeation modes from the SF and PEDOT:PSS/SF hydrogels. The accumulative drug release amounts *vs.* time can be fitted to the Korsmeyer and Peppas model[44] as in eqn (2):

$$\frac{M_t}{M_\infty} = kt^n \quad (2)$$

where $\frac{M_t}{M_\infty}$ is the fraction of accumulative drug released at time t, k is the kinetic constant (with the unit of t^{-n}), and n is the apparent diffusional scaling exponent indicative of the drug release mode. From eqn (2), the apparent diffusional scaling exponent (n) and the kinetic constant (k) can be calculated from the log–log plot of $\frac{M_t}{M_\infty}$ *versus* time.

When the apparent diffusional scaling exponent (n) is equal to 0.5, the Higuchi model can be used to determine the drug release rate as shown in eqn (3):[45]

$$\frac{M_t}{M_\infty} = k_H t^{1/2} \quad (3)$$

where k_H is the Higuchi constant (with the unit of $t^{-1/2}$). From eqn (3), the Higuchi constant (k_H) can be calculated from the slope of $\frac{M_t}{M_\infty}$ *versus* the square root of time (h) on a linear-$t^{1/2}$ plot.

The diffusion coefficient (D) can be calculated from the slope of amount of drug released *versus* the square root of time according to Higuchi's equation (eqn (4)) as follows:[45]

$$Q = \frac{M_t}{A} = 2C_0\left(\frac{D_t}{\pi}\right)^{1/2} \quad (4)$$

where M_t is the amount of drug released (mg), A is the diffusion area (cm^2), C_0 is the initial drug concentration in the matrix (mg cm^{-3}), and D is the apparent drug diffusion coefficient (cm^2 s^{-1}).

2.7.14 Statistical analysis. The drug amounts released, in the release and release-permeation experiments, were determined with at least three samples. In the swelling test, the SF and PEDOT:PSS/SF hydrogels were also investigated with three samples. The data were reported as the average ± standard deviation (SD). The statistical significance analysis between the three groups was analyzed by one-way ANOVA followed by Tukey's test using SigmaPlot software version 12.0 (Systat Software Inc.), for which the results are reported here as p-values. A p-value < 0.05 was considered to be significant and a p-value < 0.01 to be insignificant.

3. Results and discussion

3.1 Chemical structure of insulin-loaded PEDOT:PSS/SF hydrogels

PEDOT:PSS was synthesized *via* chemical oxidative polymerization following the procedure reported by Sakunpongpitiporn *et al.*, 2019. In the previous work, the structure of PEDOT:PSS was identified with two coexisting dopants, namely, PSS^-, and SO_4^{2-} ($Na_2S_2O_8$ as the oxidant). The dopants (negative charges) interacted with the PEDOT (positive charges) chain *via* the electrostatic force, whereas the sodium ion (Na^+) from the oxidant also interacted with PSS^- to form PSSNa, as shown in Fig. 1A. The PEDOT:PSS electrical conductivity was measured and found to be 1666 ± 49.08 S cm^{-1}.[35] In the case of insulin, the insulin (with the pH of 5.4) can possess either a negative or positive charge depending on the solution pH value.[46] Insulin carried a negative charge as the pH values of insulin and insulin-loaded PEDOT:PSS solutions were measured and found to be 10.63 and 9.92, respectively.[47] Therefore, insulin molecules interacted with the PEDOT chain *via* the electrostatic force and replaced some dopant PSS molecules, as shown in Fig. 1A. As the insulin molecular weight (5808 g mol^{-1}) was lower than that of PSS (75 000 g mol^{-1}) and PSS was hydrophilic, some PSS molecules were readily replaced in this process.[48]

The SF hydrogel can be formed *via* the physical crosslinking by heating, which affects the vibration mode of the molecules, enhances the frequency of molecular collisions, and promotes the aggregation of the silk fibroin molecules.[49] At a high temperature, silk I (random coil) structure can be easily transformed to silk II (beta-sheet) structure resulting in the SF chain transformation from silk I to silk II *via* the hydrogen bonds between adjacent chains or intermolecular hydrogen bonding, as shown in Fig. 1B.[50] Silk I is a metastable and unstable structure, whereas silk II is the β-sheet conformation, which is relatively a more stable structure.[51] In the case of the insulin-loaded PEDOT:PSS/SF hydrogels, insulin was incorporated between adjacent SF chains, as shown in Fig. 1B.

The cytotoxicity of 3.0% w/v SF, 5.0% w/v SF, and PEDOT:PSS_3.0% w/v SF was examined *via* the MTT cytotoxicity assay using human skin fibroblast cells, as shown in Table S3.† The percentages of cell viability of 3.0% w/v SF, 5.0% w/v SF, and PEDOT:PSS_3.0% w/v SF were found to be 87%, 90%, and 80% ($p < 0.01$), respectively. If the cell viability is less than 70% of the blank, it has a cytotoxic potential; therefore, the SF hydrogels and PEDOT:PSS/SF matrix were not toxic to the human skin.[52]

3.2 Insulin-loaded PEDOT:PSS/SF hydrogel characterizations

The FTIR spectra of the SF hydrogel, insulin, PEDOT:PSS, insulin-loaded PEDOT:PSS, insulin-loaded SF hydrogel, and insulin-loaded PEDOT:PSS/SF hydrogel are shown in Fig. 2A. The characteristic peaks of the SF hydrogel, as shown in Fig. 2A(a), can be seen at 1637 cm^{-1}, 1513 cm^{-1}, and 1233 cm^{-1} corresponding to amide I (C═O stretching) in the form of the beta sheet structure or silk II, amide II (N–H bending), and amide III (C–N stretching), respectively.[53,54]

The FTIR spectrum of insulin, as shown in Fig. 2A(b), shows peaks at 1637 cm^{-1} and 1534 cm^{-1}, which are related to amide I and amide II, respectively.[55] The main characteristic peaks of PEDOT:PSS, as shown in Fig. 2A(c), appeared at 3420 cm^{-1}, 1521 cm^{-1}, and 1314 cm^{-1}, which can be assigned to the O–H stretching vibration in PSS, the C═C stretching vibration in

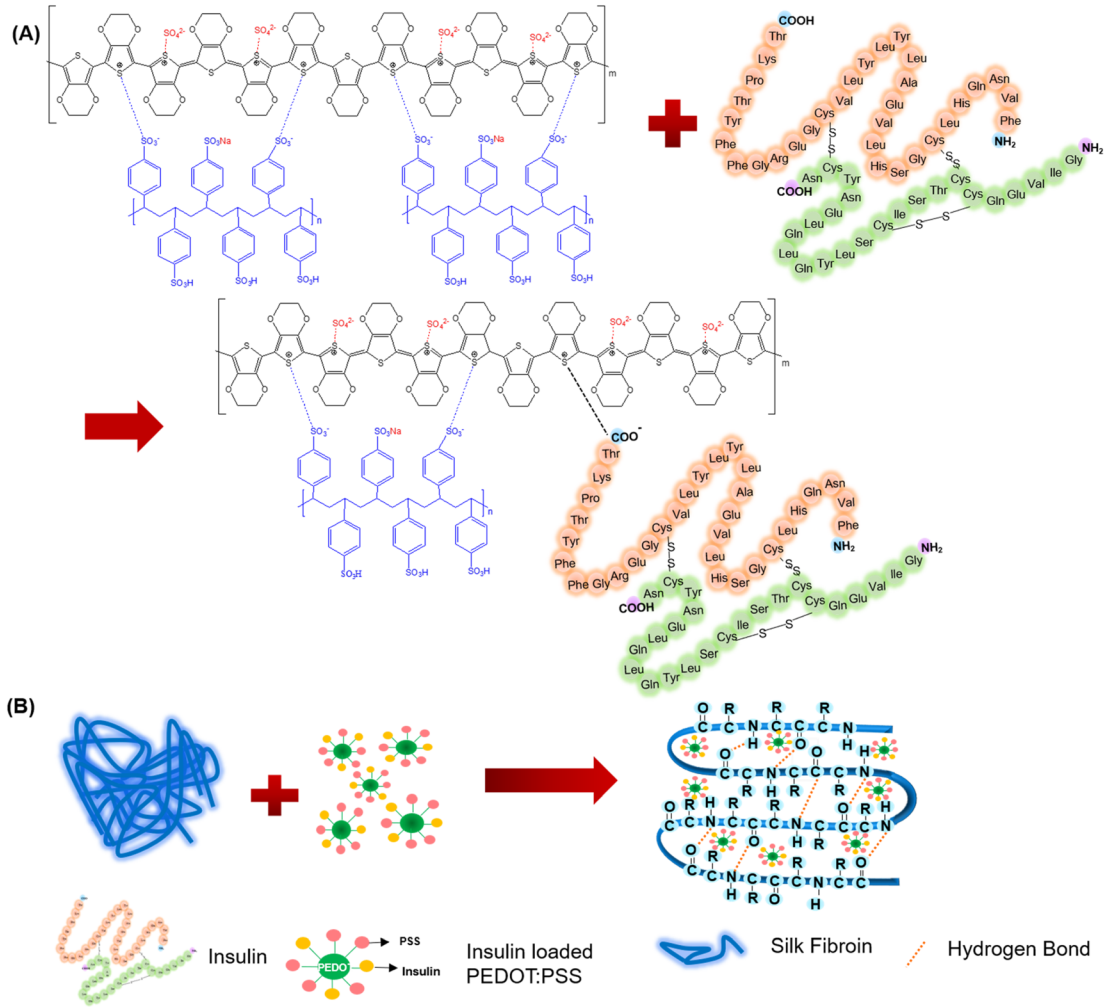

Fig. 1 Schematics of (A) insulin-loaded PEDOT:PSS and (B) transformation of the insulin-loaded PEDOT:PSS/SF hydrogel from random coil to beta-sheet crystalline.

PEDOT and PSS, and the C–C stretching vibration in PEDOT and PSS, respectively. The peaks at 1198 cm^{-1} and 1087 cm^{-1} are assigned to the S=O symmetric and asymmetric stretching vibrations from PSS and $Na_2S_2O_8$ (oxidant).[35] The peaks attributed to the O–H and S=O stretching vibrations indicate that PSS interacts with the PEDOT chain.

The main characteristic peaks of insulin-loaded PEDOT:PSS, as shown in Fig. 2A(d), are at 3429 cm^{-1}, 1654 cm^{-1}, and 1512 cm^{-1} corresponding to the incorporated N–H (insulin) and the O–H (PSS) stretching vibration, the C=O stretching vibration (insulin), the incorporated N–H bending vibration (insulin) and the C=C stretching vibration (PEDOT and PSS). The main peaks of insulin-loaded PEDOT:PSS when compared to PEDOT:PSS show the shifts from 3420 cm^{-1} to 3429 cm^{-1}, and 1521 cm^{-1} to 1512 cm^{-1}. The shifts confirmed that insulin was successfully loaded and interacted with PEDOT:PSS.

The FTIR spectrum of the insulin-loaded SF hydrogel, as shown in Fig. 2A(e), exhibits the main characteristic peaks at 1618 cm^{-1}, 1512 cm^{-1}, and 1230 cm^{-1}, which can be assigned to amide I (strong intermolecular beta-sheet), amide II, and amide III, respectively.[56] This suggests that insulin interacted with the SF chain *via* hydrogen bonding, while the SF hydrogel still retained the beta sheet structure (silk II).[38]

The FTIR spectrum of the insulin-loaded PEDOT:PSS/SF hydrogel, as shown in Fig. 2A(f), demonstrates the peaks at 3279 cm^{-1}, 1622 cm^{-1}, 1514 cm^{-1}, 1125 cm^{-1} and 1063 cm^{-1}, which are related to the N–H stretching vibration, C=O stretching vibration, N–H bending vibration, and S=O symmetric and asymmetric stretching vibration.[35,56] These peaks confirm that insulin was successfully loaded in the PEDOT:PSS/SF hydrogel, while the SF hydrogel still retained the beta sheet structure (silk II).[56]

The thermal stability of the SF hydrogel, insulin, PEDOT:PSS, insulin-loaded PEDOT:PSS, insulin-loaded SF hydrogel, and insulin-loaded PEDOT:PSS/SF hydrogel is shown in Fig. 2B. The thermogram of the SF hydrogel, as shown in Fig. 2B(a), has 2 decomposition stages: 40–180 °C is the loss of moisture and water; and 180–800 °C is the cleavage of peptide bonds.[57] T_d of SF hydrogel is at 299 °C, which is similar to previous works: 307 °C (ref. 58) and 295 °C.[59] The result indicates that the structure of SF hydrogel is the beta-sheet structure or silk II.[60]

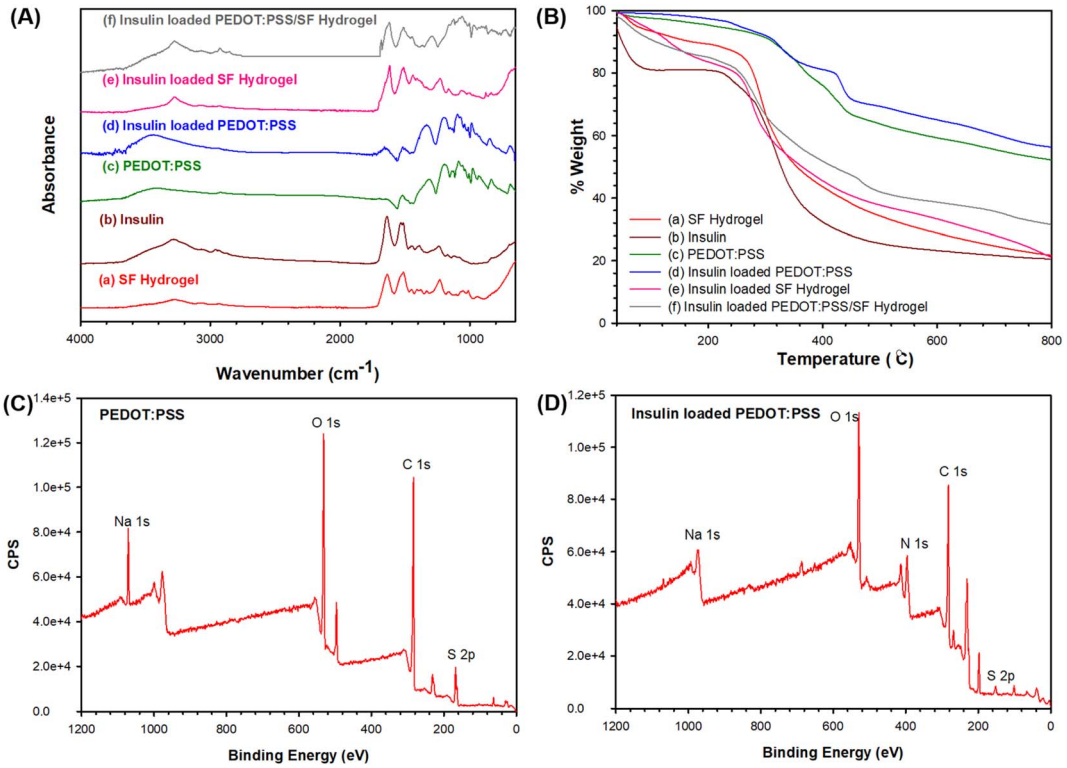

Fig. 2 Characterizations: (A) FTIR spectra; (B) TGA; (C) survey-scan of PEDOT:PSS; and (D) survey-scan of insulin-loaded PEDOT:PSS.

The thermogram of insulin powder for the unmodified commercial human insulin powder is shown in Fig. 2B(a) and S1a.† It shows 2 decomposition stages at 40–100 °C and 180–800 °C, which are assigned to the loss of water and the decomposition of protein.[61] T_d of insulin powder is 313 °C, which is close to the previous work of 318 °C.[62]

The thermogram of PEDOT:PSS, as shown in Fig. 2B(c) and S1b,† demonstrates 3 decomposition stages: 40–160 °C is the evaporation of water; 160–390 °C is the decomposition of PSS and side chains; and 390–800 °C is the decomposition of the polymer backbone.[63] The T_d values of PSS and PEDOT are 360 °C and 428 °C whereas the weight losses are 18.35% and 19.23%, respectively.

The thermogram of insulin-loaded PEDOT:PSS, as shown in Fig. 2B(d) and S1c,† is similar to that of PEDOT:PSS, but it shows a new decomposition stage of individual insulin particles at 200–290 °C. T_d of insulin, PSS, and PEDOT are 250 °C, 326 °C, and 414 °C with the corresponding weight losses of 4.13%, 12.33%, and 17.27%, respectively. The T_d value of PEDOT of insulin-loaded PEDOT:PSS shifted to a lower temperature than that of pristine PEDOT:PSS. A possible reason is that the insulin molecules interacted with the PEDOT chains, leading to the replacement of PSS molecules as the counter ions, as verified by the decrease in the % weight loss of PSS and the XPS data. Thus, insulin was successfully loaded in PEDOT:PSS, consistent with the FTIR result.

The thermogram of insulin-loaded SF hydrogel, as shown in Fig. 2B(e), demonstrates 2 decomposition stages which are similar to the SF hydrogel. The T_d value of insulin of the insulin-loaded SF hydrogel shifted from 299 °C to 278 °C, confirming that insulin was successfully loaded into the SF hydrogel.[38]

The thermogram of the insulin-loaded PEDOT:PSS/SF hydrogel, as shown in Fig. 2B(f), shows 4 decomposition stages, which are similar to the thermograms of the insulin-loaded PEDOT:PSS and the insulin-loaded SF hydrogel. The T_d values of the insulin-loaded PEDOT:PSS/SF hydrogel are 283 °C, 329 °C, and 419 °C, which can be assigned to the decompositions of insulin and the SF hydrogel combined, PSS, and PEDOT backbone, respectively. From the results, the TGA and FTIR data are consistent; individual insulin molecules were successfully loaded into PEDOT:PSS, resulting in insulin-loaded PEDOT:PSS to be successfully incorporated into the SF hydrogel.

The survey scan XPS spectrum of PEDOT:PSS (Fig. 2C) demonstrates C 1s (63.35%), O 1s (27.02%), S 2p (5.91%), and Na 1s (3.73%), which are located at 284 eV, 523 eV, 168 eV, and 1071 eV, respectively.[35] The existence of these elements indicates that the elements of PEDOT:PSS are consistent with the structure, as shown in Fig. 1A. The survey scan XPS spectrum of insulin-loaded PEDOT:PSS (Fig. 2D) shows C 1s (56.64%), O 1s (23.94%), S 2p (1.07%), Na 1s (0.38%), and N 1s (17.97%) which are located at 282 eV, 529 eV, 159 eV, 1069 eV, and 396 eV, respectively. The existence of N 1s from insulin and shifting of S 2p from 168 eV to 159 eV suggest that insulin molecules reacted with the PEDOT chain, as shown in Fig. 1A.[64] The decreases of S 2p and Na 1s imply that some dopant PSS molecules were replaced with insulin molecules.

The deconvolutions of S 2p of PEDOT:PSS and insulin-loaded PEDOT:PSS from the narrow scan XPS spectra are

shown in Fig. S2 and Table S2.† For PEDOT:PSS, as shown in Fig. S2(a),† the S 2p peaks of PEDOT, PSS^- and SO_4^{2-}, and PSSNa spectra are located at 164.25 and 165.54 eV, 168.27 and 169.68 eV, and 169.09 and 170.48 eV, where the *S* amounts of the three components are 33.43%, 45.07%, and 21.49%, respectively.[35] For insulin-loaded PEDOT:PSS, as shown in Fig. S2(b),† the S 2p peaks of PEDOT, PSS^- and SO_4^{2-}, and PSSNa spectra are located at 165.11 and 166.39 eV, 169.24 and 170.73 eV, and 170.06 and 171.50 eV, where the *S* amounts of PEDOT, PSS^- and SO_4^{2-}, and PSSNa are 47.87%, 36.45%, and 15.68%, respectively. The S 2p peaks of insulin-loaded PEDOT:PSS shifted to higher binding energy values when compared to PEDOT:PSS. The shifting in the binding energy peaks, the relative *S* amount increase in PEDOT, and the relative *S* amount decreases in (PSS^- and SO_4^{2-}) and PSSNa suggest that the insulin molecules interacted with the PEDOT chain *via* the electrostatic force replacing some PSS molecules, leading to the *S* amount decrease in PSSNa. From the results, the FTIR, TGA, and XPS data are consistent. They suggest that the insulin molecules interacted with the PEDOT chain and replaced with some PSS molecules, leading to a decrease of PSSNa.

3.3 Swelling behaviors of SF and PEDOT:PSS/SF hydrogels

The swelling behaviors of the SF and PEDOT:PSS/SF hydrogels in terms of the swelling times to equilibrium, the percentages of swelling, and the mesh sizes with and without electric voltages are shown in Table S4.† For the effect of SF concentrations, the percentage of swelling at 3% w/v SF, 4% w/v SF, and 5% w/v SF are 111 ± 16, 93 ± 12, and 61 ± 13 (p value < 0.01), while the times to equilibrium are 90 min, 100 min, and 110 min, respectively. The mesh sizes at 3% w/v SF, 4% w/v SF, and 5% w/v SF are 13.7 Å, 12.8 Å, and 12.3 Å, respectively. At higher SF concentrations, they possess higher degrees of entanglement, leading to a decrease in the percentage of swelling and mesh size, and an increase in the swelling time to equilibrium.[65,66] Under the effect of electric voltages, the percentages of swelling of 3% w/v SF at 3.0 V and 6.0 V are 140 ± 21 and 154 ± 19 (p value < 0.05), whereas the times to equilibrium and mesh sizes are 85 min and 75 min, and 48.8 Å and 63.8 Å respectively. The percentage of swelling and mesh size increased while the time to equilibrium decreased, consistent with previous works.[67,68] At higher electric voltages, the matrix expansion occurred because of the electro-repulsive force between the cathode electrode and the SF chain (pI of SF = 4.53).[69,70]

For the effect of PEDOT:PSS/SF concentrations, the percentages of swelling at a pH of 7.4 of the PEDOT:PSS_3% w/v SF, 4% w/v SF, and 5% w/v SF are 850 ± 26, 787 ± 53, and 573 ± 76 (p value < 0.01), whereas the times to equilibrium are 70 min, 90 min, and 100 min, respectively. The mesh sizes of PEDOT:PSS_3% w/v SF, 4% w/v SF, and 5% w/v SF are 26.5 Å, 21.1 Å, and 19.7 Å, respectively. Adding PEDOT:PSS in the SF hydrogels produced higher percentages of swelling and mesh sizes, and lowered the swelling time to equilibrium, as PEDOT:PSS was a hydrophilic polymer and was incorporated into the SF hydrogel leading to a higher free volume.[71] At higher PEDOT:PSS/SF concentrations, the degree of swelling and mesh size decreased, whereas the swelling time to equilibrium increased due to the higher entanglement or denser cross-linking network.[72]

For the effect of pH values, the percentages of swelling of PEDOT:PSS_3% w/v SF at pH values 5.5 and 7.4 are 652 ± 18 and 850 ± 26 (p value < 0.01), respectively. At a lower pH, SF possesses a lower amount of negative charge (SF pI = 4.53), leading to lower mesh size and less matrix expansion.[46,69] Under the effect of electric voltages, the percentages of swelling of PEDOT:PSS_3% w/v SF hydrogel at 0 V, 3 V, and 6 V are 850 ± 26, 964 ± 62, and 1137 ± 30 (p value < 0.01), while the swelling times to equilibrium are 70 min, 50 min, and 40 min, respectively. The mesh size increased from 26.5 Å (0 V) to 473.2 Å (6 V). At a higher electric voltage, the degree of swelling and mesh size increased but the swelling time to equilibrium decreased due to the PEDOT:PSS/SF expansion from the electro-repulsive force between the cathode and the SF chain.[30]

3.4 Morphology

The surface morphology of PEDOT:PSS, insulin powder, insulin-loaded PEDOT:PSS, 3.0% w/v SF hydrogel, insulin-loaded SF hydrogel, and insulin-loaded PEDOT:PSS/SF hydrogel was investigated by SEM, as shown in Fig. 3. The PEDOT:PSS (Fig. 3a) demonstrates the smooth and homogeneous surfaces. The insulin powder (Fig. 3b) shows the aggregated particles of irregular shapes.[73] Insulin-loaded PEDOT:PSS, as shown in Fig. 3c, shows a rougher surface than PEDOT:PSS alone. This indicates that isolated insulin molecules or individual insulin particles are incorporated with PEDOT:PSS. The 3.0% w/v SF hydrogel, as shown in Fig. 3d, shows a smooth surface.[74,75] The insulin-loaded SF hydrogel (Fig. 3e) also shows a smooth surface. The insulin-loaded PEDOT:PSS/SF hydrogel (Fig. 3f) shows a surface roughness, implying that the insulin-loaded PEDOT:PSS was incorporated into the SF hydrogel. The results from SEM images, FTIR, TGA, and XPS data are consistent with each other. They confirm that insulin was successfully loaded in PEDOT:PSS, and the insulin-loaded PEDOT:PSS was incorporated into the SF hydrogel.

The cross-section morphology of SF hydrogels after swelling with and without electric voltages is demonstrated in Fig. 4. All of SF hydrogels show the porous structures with interconnected pores.[76] At higher SF concentrations (Fig. 4a–c), the pore size

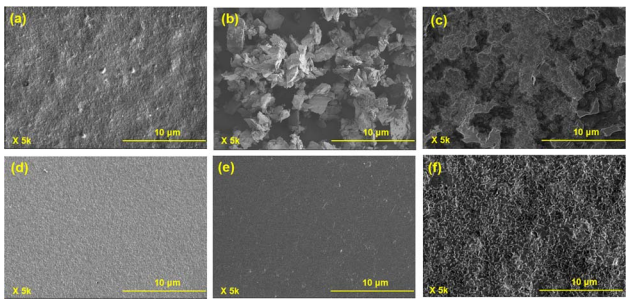

Fig. 3 SEM surface images: (a) PEDOT:PSS; (b) insulin powder; (c) insulin-loaded PEDOT:PSS; (d) 3.0% w/v SF hydrogel; (e) insulin-loaded SF hydrogel; and (f) insulin-loaded PEDOT:PSS/SF hydrogels.

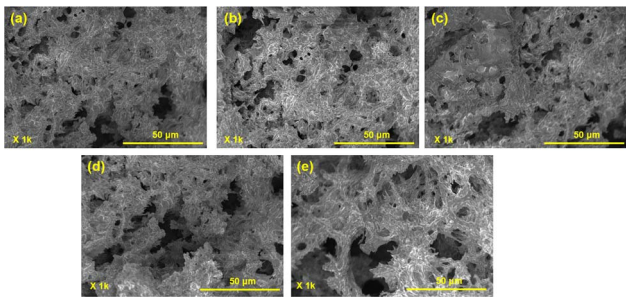

Fig. 4 Cross-section SEM images of SF hydrogels after swelling with and without electric voltages: (a) 3.0% w/v; (b) 4.0% w/v; (c) 5.0% w/v; (d) 3.0% w/v at $E = 3.0$ V; and (e) 6.0% w/v at $E = 6.0$ V.

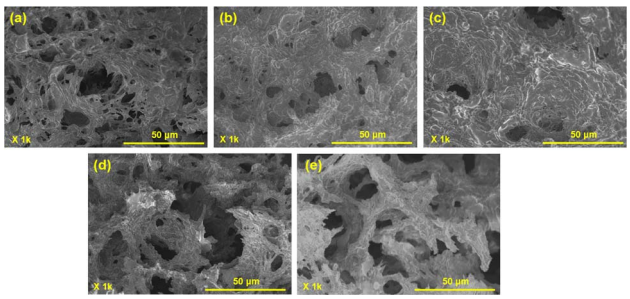

Fig. 5 Cross-section SEM images of PEDOT:PSS/SF hydrogels after swelling with and without electric voltages: (a) 3.0% w/v; (b) 4.0% w/v; (c) 5.0% w/v; (d) 3.0% w/v at $E = 3.0$ V; and (e) 3.0% w/v at $E = 6.0$ V.

decreased due to a denser crosslinking network.[66] At higher electric voltages (Fig. 4d and e), the pore size increased due to the electro-repulsive force between the cathode and the SF chain (pI of SF = 4.53), leading to the SF expansion.[30,69]

The cross-section morphology of PEDOT:PSS/SF hydrogels after swelling with and without electric voltages is shown in Fig. 5. All samples show porous structures with interconnected pores. The addition of PEDOT:PSS in the SF hydrogel produced larger pore sizes relative to the pristine SF hydrogel as PEDOT:PSS was miscible with and can be easily incorporated into the SF hydrogel, leading to an increase in the distance between crosslinked points and high mesh sizes.[77] At higher % w/v of SF in the PEDOT:PSS/SF hydrogels (Fig. 5a–c), the pore size decreased because of the denser crosslinking network.[65] At higher electric voltages (Fig. 5a, d and e), the pore size increased due to the electro-repulsive force between the cathode and the SF chain.[30]

3.5 Release behavior

3.5.1 Actual drug amounts. For the insulin and insulin-loaded PEDOT:PSS/SF hydrogels (thickness = 0.15 mm, area = 3.14 cm^2), the actual drug amounts loaded were determined by UV-vis, as tabulated in Table 1. The actual drug amounts loaded into the 3.0% w/v SF, 4.0% w/v SF, and 5.0% w/v SF hydrogels were measured and found to be 1.03 ± 0.01 mg, 1.01 ± 0.01 mg, and 1.00 ± 0.02 mg (p value < 0.01), respectively. The actual drug amounts loaded into the PEDOT:PSS_3.0% w/v SF,

Table 1 Kinetic factors and diffusion coefficients of insulin released from SF hydrogels and PEDOT:PSS/SF hydrogels, at different electric voltages, with a matrix thickness of 0.15 ± 0.03 mm and an area of 3.14 cm^2[a]

Conditions (actual drug (mg))	pH	Electric voltage (V)	Power law			Higuchi			Amount of insulin released (mg)	C_0 (g cm^{-3})	% release	Time to equilibrium (h)
			n	k	r^2	k_H	r^2	D (cm^2 s^{-1})				
3.0% w/v SF (1.03 ± 0.01)	7.4	—	0.53	2.97×10^{-3}	0.94	3.10×10^{-3}	0.91	7.00×10^{-10}	0.72	0.023	60.0	12
	7.4	3.0 (2.31 μA)	0.45	7.56×10^{-3}	0.92	2.95×10^{-3}	0.86	7.60×10^{-10}	0.78	0.023	64.7	9
	7.4	6.0 (3.12 μA)	0.41	1.15×10^{-2}	0.92	2.87×10^{-3}	0.87	1.13×10^{-9}	0.96	0.023	73.1	8
4.0% w/v SF (1.01 ± 0.01)	7.4	—	0.51	3.78×10^{-3}	0.91	3.03×10^{-3}	0.89	4.52×10^{-10}	0.58	0.023	48.7	13
5.0% w/v SF (1.00 ± 0.02)	7.4	—	0.45	7.78×10^{-3}	0.85	2.80×10^{-3}	0.85	2.56×10^{-10}	0.47	0.023	39.4	14
PEDOT:PSS_3.0% w/v SF (1.07 ± 0.01)	7.4	—	0.40	1.22×10^{-2}	0.90	2.79×10^{-3}	0.86	7.26×10^{-10}	0.80	0.023	66.3	8
	7.4	3.0 (2.81 μA)	0.50	4.39×10^{-3}	0.93	3.03×10^{-3}	0.90	1.14×10^{-9}	0.93	0.023	77.3	7
	7.4	6.0 (4.13 μA)	0.51	3.87×10^{-3}	0.90	3.04×10^{-3}	0.87	1.29×10^{-9}	0.98	0.023	81.9	6
PEDOT:PSS_4.0% w/v SF (1.05 ± 0.01)	7.4	—	0.42	2.57×10^{-3}	0.87	2.89×10^{-3}	0.79	6.49×10^{-10}	0.73	0.023	60.5	9
PEDOT:PSS_5.0% w/v SF (1.08 ± 0.01)	7.4	—	0.44	7.82×10^{-3}	0.92	2.93×10^{-3}	0.87	3.83×10^{-10}	0.55	0.023	46.2	10

[a] The p values of actual drug amounts for effects of SF concentrations (3.0%, 4.0%, and 5.0% w/v SF), and PEDOT:PSS/SF concentrations (PEDOT:PSS_3.0%, 4.0%, and 5.0% w/v SF) were <0.01, and <0.01, respectively.

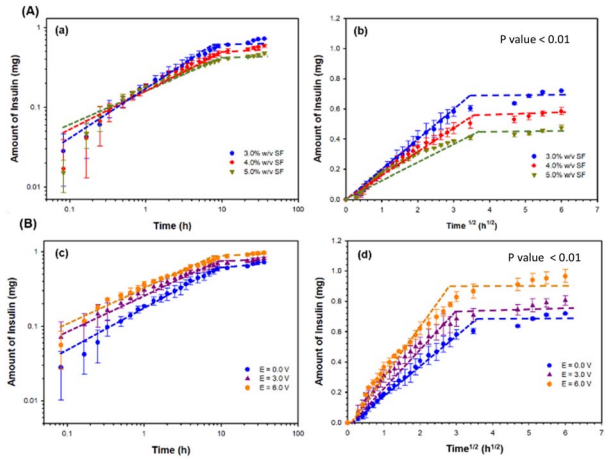

Fig. 6 Amounts of insulin released from insulin-loaded SF hydrogels under the effects of (A) SF concentrations, and (B) electric voltages with 3.0% w/v SF. (a) and (c) Amounts *versus* time in the log–log plots, and (b) and (d) amounts *versus* time$^{1/2}$.

PEDOT:PSS_4.0% w/v SF, and PEDOT:PSS_5.0% w/v SF hydrogels were 1.07 ± 0.01 mg, 1.05 ± 0.01 mg, and 1.08 ± 0.01 mg (p value < 0.01), respectively.

3.5.2 Release kinetics of insulin from SF and PEDOT:PSS/SF hydrogels. In the case of insulin-loaded SF hydrogels, the release profiles under the effects of SF % w/v and electric voltages are shown in Fig. 6A(a) and B(c), respectively. The apparent scaling exponents (n) in eqn (2) were determined from the slopes of the log–log plot between M_t/M_∞ and t under the effects of SF concentrations and electric voltages, as tabulated in Table 1. Under the effects of SF concentrations and electric voltages, the n values are between 0.41 and 0.53, as tabulated in Table 1. The release modes can be classified into the case-I transport or the Fickian diffusion mode.[44,78]

In the case of the insulin-loaded PEDOT:PSS/SF hydrogels, the release profiles under the effects of SF % w/v and electric voltages are shown in Fig. 7A(a) and B(c), respectively. Under the effects of SF concentrations and electric voltages, the n values are between 0.40 and 0.51, as tabulated in Table 1. The release modes can also be classified into the case-I transport or the Fickian diffusion mode.[44,78]

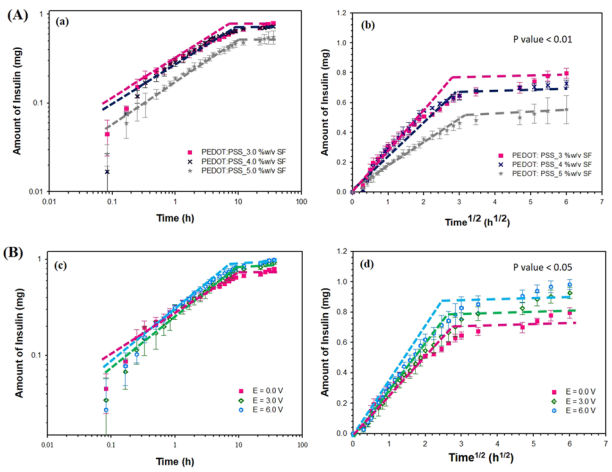

Fig. 7 Amounts of insulin released from insulin-loaded PEDOT:PSS/SF hydrogels under the effects of (A) SF concentrations and (B) electric voltages with PEDOT:PSS_3.0% w/v SF. (a and c) Amounts *versus* time in the log–log plots, and (b and d) amounts *versus* time$^{1/2}$.

3.5.3 *In vitro* drug-release

3.5.3.1 Insulin-loaded SF hydrogels. The amounts of insulin released from the insulin-loaded SF hydrogels under the effect of SF concentrations are tabulated in Table 1. The amounts of insulin released are 60.0%, 48.7%, and 39.4% (p value < 0.01) for the 3.0% w/v SF, 4.0% w/v SF, and 5.0% w/v SF hydrogels, respectively. At higher SF concentrations, the time to equilibrium increased from 12 h to 14 h while the diffusion coefficient (D) decreased from 7.00 × 10^{-10} cm^2 s^{-1} to 2.56 × 10^{-10} cm^2 s^{-1}. A higher SF % w/v provided a denser crosslinking network or a higher degree of entanglement, resulting in a smaller mesh size.[66]

The amounts of insulin released from the insulin-loaded SF hydrogels under the effect of electric voltages are tabulated in Table 1. The amounts of insulin released from the 3.0% w/v SF hydrogel are 60.0%, 64.7%, and 73.1% (p value < 0.01) at 0 V, 3 V, and 6 V, respectively. The time to equilibrium decreased from 12 h to 8 h, whereas the apparent diffusion coefficient (D) increased from 7.00 × 10^{-10} cm^2 s^{-1} to 1.13 × 10^{-9} cm^2 s^{-1}, respectively. At a higher electric voltage, the increases in the amount of insulin released and diffusion coefficient resulted from the higher electro-repulsive force between the cathode and insulin, the SF chain, the electroosmosis, and the SF matrix expansion.[31]

3.5.3.2 Insulin-loaded PEDOT:PSS/SF hydrogels. The amounts of insulin released from the insulin-loaded PEDOT:PSS/SF hydrogels under the effect of SF concentrations are tabulated in Table 1. For the PEDOT:PSS_3% w/v SF, PEDOT:PSS_4% w/v SF, and PEDOT:PSS_5% w/v SF hydrogels, the amounts of insulin released are 66.3%, 60.5%, and 46.2% (p value < 0.01), respectively. At higher SF concentrations, the time to equilibrium increased from 8 h to 10 h, while the diffusion coefficient (D) decreased from 7.26 × 10^{-10} cm^2 s^{-1} to 3.83 × 10^{-10} cm^2 s^{-1}. Relative to the case of pristine SF hydrogel, the addition of PEDOT:PSS provided only moderate increases in the amount of insulin released and the diffusion coefficient, and the decrease in the time to equilibrium. The PEDOT:PSS molecules incorporated into the SF hydrogels induced the partial matrix swelling, leading to higher mesh sizes consistent with the data, as tabulated in Table S4,†[77] whereas the effect of drug carrier host is not apparent here without the electric voltage.

The amounts of insulin released from the insulin-loaded PEDOT:PSS_3% w/v SF hydrogel under the effect of electric voltages are tabulated in Table 1. The amounts of insulin released and the diffusion coefficients at 0 V, 3 V, and 6 V are 66.3%, 77.3%, and 81.9% (p value < 0.05) and 7.00 × 10^{-10} cm^2 s^{-1}, 1.14 × 10^{-9} cm^2 s^{-1}, and 1.29 × 10^{-9} cm^2 s^{-1}, respectively. The time to equilibrium decreased from 8 hours to 6 hours. At a higher electrical voltage, the amount of insulin released and the diffusion coefficient increased, while the time to equilibrium decreased. The individual insulin molecules attached to

the PEDOT:PSS molecules were released from the SF hydrogel matrix by the possible four mechanisms: the insulin concentration gradient in the initial period; the electro-repulsive force between the cathode and the insulin molecules; the electroosmosis; and lastly, the PEDOT:PSS_3% w/v SF expansion from the electro-repulsive force between the cathode and the SF chains presumably in the later period.[38,47]

3.6 Release-permeation behavior

3.6.1 Release kinetics of insulin from PEDOT:PSS/SF hydrogels. The release-permeation profiles of insulin under the effects of pH values and electric voltages from insulin-loaded PEDOT:PSS_3.0% w/v SF are shown in Fig. 8A(a) and B(c), respectively. The apparent scaling exponents (n) in eqn (2) were calculated from the slope of the log–log plot between M_t/M_∞ and t under the effects of pH values and electric voltages, as tabulated in Table 2. For the effects of pH values and electric voltages, the n values are between 0.42 and 0.62. The release-permeation modes can also be classified into the case-I transport or the Fickian diffusion mode.[44,78]

3.6.2 *In vitro* release-permeation. The amounts of insulin release-permeation from the insulin-loaded PEDOT:PSS_3.0% w/v SF hydrogels under the effect of pH values are tabulated in Table 2. At pH values of 5.5 and 7.4, the amounts of insulin released and the apparent diffusion coefficients (D) are 48.4% to 56.8% (p value < 0.01) and 4.31×10^{-10} cm^2 s^{-1} to 5.35×10^{-10} cm^2 s^{-1} respectively. The time to equilibrium decreased from 12 h to 10 h. At a pH of 5.5, the amount of insulin release-permeation and the diffusion coefficient are lower; this was possibly due to the lower matrix swelling as both insulin and SF chains possessed lesser negative charges (SF pI = 4.53, insulin pI = 5.4).[46,47,69,79] The fluid lipid bilayer membrane (pig belly skin) requires a longer time to create an aqueous pathway or pore called 'the pore formation period'.[80] The effect of pH values may presumably influence the membrane pore formation.

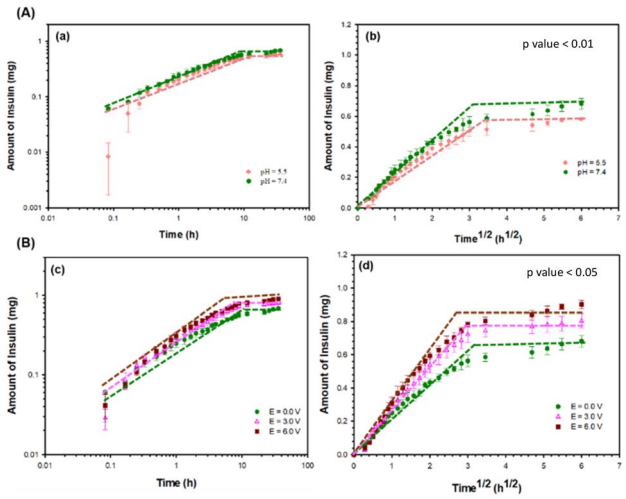

Fig. 8 Amounts of insulin release-permeation from insulin-loaded PEDOT:PSS_3.0% w/v SF hydrogels under the effects of (A) pH values and (B) electric voltages. (a and c) Amounts *versus* time in the log–log plots, and (b and d) amounts *versus* time$^{1/2}$.

Table 2 Kinetic factors and diffusion coefficients of insulin release-permeation from the PEDOT:PSS_3.0% w/v SF hydrogels, at different pH values and electric voltages, with a matrix thickness of 0.15 ± 0.03 mm and an area of 3.14 cm^2

Conditions (actual drug (mg))	pH	Electric voltage (V)	Power law			Higuchi		D (cm^2 s^{-1})	Amount of insulin released (mg)	C_0 (g cm^{-3})	% release	Time to equilibrium (h)
			n	k	r^2	k_H	r^2					
PEDOT:PSS_3.0% w/v SF (1.07 ± 0.01)	5.5	—	0.42	1.38×10^{-3}	0.86	2.97×10^{-3}	0.84	4.31×10^{-10}	0.58	0.023	48.4	12
	7.4	—	0.46	7.93×10^{-3}	0.98	2.85×10^{-3}	0.87	5.35×10^{-10}	0.68	0.023	56.8	10
	7.4	3.0 (2.21 μA)	0.58	2.74×10^{-3}	0.93	2.87×10^{-3}	0.87	8.35×10^{-10}	0.80	0.023	67.0	9
	7.4	6.0 (3.12 μA)	0.62	1.83×10^{-3}	0.97	2.99×10^{-3}	0.84	1.06×10^{-9}	0.90	0.023	75.2	8

The amounts of insulin release-permeation from the insulin loaded PEDOT:PSS_3.0% w/v SF hydrogel under the effect of electric voltages are tabulated in Table 2. At electric voltages of 0 V, 3 V, and 6 V, the amounts of insulin release-permeation and the diffusion coefficients (D) are 56.8%, 67.0%, and 75.2% (p value < 0.05) and 5.35×10^{-10} cm^2 s^{-1}, 8.35×10^{-10} cm^2 s^{-1}, and 1.06×10^{-9} cm^2 s^{-1}, respectively. The time to equilibrium decreased from 10 h to 8 h. At a higher electric voltage, the amount of insulin release-permeation and the diffusion coefficient (D) increased due to the insulin concentration gradient in the initial period, a higher electro-repulsive force between the cathode and the insulin molecules, the electroosmosis, and the partial PEDOT:PSS/SF hydrogel expansion.[38,47] Here the effect of electric voltage on the release-permeation is more drastic than the pH experiment.

The dosage of basal insulin for treating diabetes patients (average weight is 98.9 ± 1.5 kg (ref. 81)) is 27.2 units or 0.94 mg (1 unit of insulin is 0.0347 mg (ref. 82)) during a period of 24 h.[83] In the release experiment, the amounts of insulin release from the 3.0% w/v SF and PEDOT:PSS_3.0% w/v SF hydrogels were between 0.72 and 0.96 mg (12–8 h) and 0.80 and 0.98 mg (8–6 h) at electric voltages between 0 and 6 volts. In the release-permeation, the amounts of insulin release from the PEDOT:PSS_3.0% w/v SF hydrogel were between 0.68 and 0.90 mg, while the time to equilibrium was 10–8 h at electric voltages between 0 and 6 volts. This suggests that the SF and PEDOT:PSS/SF hydrogels are potential and applicable to be used as the matrices, twice in a 24 h period, for the basal insulin dosage.

In previous works, Siddiqui *et al.* (1987) have investigated the insulin release-permeation *via* electric field by using a hairless rat skin (350–450 g). At a pH of 7.1, the blood glucose without electric field decreased by less than 5%, while it decreased by 55% at an electric field of 9 V and 4 mA.[84] Kagatani *et al.* (1997) investigated the insulin release from a poly(-dimethylaminopropylacrylamide) (PDMAPAAA) gel with rat skin. The insulin loaded in PDMAPAAA (electroresponsive) gel was injected into a rat. Under the electric field (1 mA, 0.36 mA cm^{-2}), the blood glucose concentration decreased by 30% in 1 h.[85] Kajimoto *et al.*, 2011 investigated the release of insulin encapsulated by liposomes using rat skin as the membrane under electric field. Under the electric field (0.45 mA cm^{-2}), the blood glucose level slowly decreased by 20% and showed a basal (constant) level after 18 hours.[86] Pagneux *et al.*, 2020 investigated the insulin release from an electrothermal patch. The rGO-coated gold nanohole-modified Kapton (K/Au NHs), human hepatic HepG2 cell line, and fresh mouse skin were used as the electrothermal patch, matrix for release, and matrix for release-permeation, respectively. After 10 min, the amount of insulin released increased from 2 μg (0 V) to 32 μg (1.6 V) with the increasing electric field. For the release-permeation, the amount of insulin release-permeation and insulin flux after 2 hours were 23 ± 2 μg and 15.6 ± 1.3 μg cm^{-2} h^{-1}.[87] Tari *et al.*, 2021 investigated the insulin release-permeation from water-soluble polypyrrole nanoparticles (WS-PPyNPs) *via* iontophoresis using rat skin as the membrane. The cumulative amounts of permeated insulin per area at 48 hours without any electric field, anodal iontophoresis, and cathodal iontophoresis were 17.9 ± 4.69 μg cm^{-2}, 520 ± 136 μg cm^{-2}, and 835 ± 219 μg cm^{-2}, respectively.[47]

4. Conclusion

PEDOT:PSS has been successfully synthesized *via* chemical oxidative polymerization. PEDOT:PSS has been successfully attached with insulin molecules, as confirmed by FTIR, TGA, and XPS results. The SF and PEDOT:PSS/SF hydrogels were prepared and investigated for swelling under the effects of SF concentrations and electric voltages. The degree of swelling and mesh size of SF hydrogels increased with the decrease in SF concentrations due to the looser crosslinking network and higher free volume, and the fact that PEDOT:PSS was miscible with and can be easily incorporated with the SF chain. The release and release-permeation modes were classified to be the case-I transport or the Fickian diffusion mode. The insulin release and release-permeation mechanisms were the insulin concentration gradient in the initial period, the continuous electro-repulsive force between the cathode and the insulin molecules, the electroosmosis, and the partial SF hydrogel swelling from the electrostatic interaction in the latter period. At a higher pH value, insulin-loaded PEDOT:PSS possessed higher amounts of negative charges, leading to higher electro-repulsive forces between the negatively charged SF chains and insulin-loaded PEDOT:PSS. The application of electric field coupled with PEDOT:PSS as the drug carrier appeared to be the most influential cause for the insulin release-permeation, relative to other factors, namely, % w/v SF and pH values. Thus, this work demonstrated a new non-toxic and biocompatible drug-matrix hydrogel system, with PEDOT:PSS as the drug carrier and SF as the hydrogel matrix, to deliver insulin transdermally *via* iontophoresis with the controllable release rate, amount, and duration.

Author contributions

Phimchanok Sakunpongpitiporn: conceptualization, validation, methodology, funding acquisition, formal analysis, investigation, writing. Rawita Morarad: methodology, investigation. Witthawat Naeowong: conceptualization, supervision. Sumonman Niamlang: conceptualization, writing – review & editing. Anuvat Sirivat: conceptualization, funding acquisition, writing – review & editing, supervision.

Conflicts of interest

There are no conflicts to declare.

Acknowledgements

The authors would like to acknowledge the following financial support: the Royal Golden Jubilee PhD Program (RGJ PHD/0108/2559); the Conductive and Electroactive Polymer Research Unit of Chulalongkorn University; the 90th Anniversary of Chulalongkorn University Fund

(Ratchadaphiseksomphot Endowment Fund); the Thailand Science Research and Innovation Fund of Chulalongkorn University (TSRI-CU); and the National Research Council of Thailand (NRCT).

References

1 J. Zhao, G. Xu, X. Yao, H. Zhou, B. Lyu, S. Pei and P. Wen, *Drug Delivery Transl. Res.*, 2021, **12**, 2403–2427.
2 A. Panchal, V. Shah and U. M. Upadhyay, *Int. J. Res. Pharm. Sci.*, 2011, **2**, 484–492.
3 G. Sharma, A. R. Sharma, J. S. Nam, G. P. C. Doss, S. S. Lee and C. Chakraborty, *J. Nanobiotechnol.*, 2015, **13**, 74.
4 R. Zhao, Z. Lu, J. Yang, L. Zhang, Y. Li and X. Zhang, *Front. Bioeng. Biotechnol.*, 2020, **8**, 880.
5 J. Belmin and P. Valensi, *Drugs Aging*, 2003, **20**, 303–312.
6 R. B. Shah, M. Patel, D. M. Maahs and V. N. Shah, *Int. J. Pharm. Invest.*, 2016, **6**, 1–9.
7 S. Adepu and S. Ramakrishna, *Molecules*, 2021, **26**, 5905.
8 P. Bala, S. Jathar, S. Kale and K. Pel, *J. Pharm. Res.*, 2014, **8**, 1805–1835.
9 A. Kumar and K. Kumar, *J. Drug Delivery Ther.*, 2022, **10**, 98–104.
10 D. J. Kajal Sharma, V. Pandit and M. S. Ashawat, *J Posit. Sch. Psychol.*, 2022, **8**, 8882–8892.
11 W. Y. Jeong, M. Kwon, H. E. Choi and K. S. Kim, *Biomater. Res.*, 2021, **25**, 24.
12 A. Stanekzai, C. K. Sudhakar, A. M. Zhafar and V. S. Karan, *Res. J. Pharm. Technol.*, 2019, **12**, 4550–4558.
13 M. B. Brown, G. P. Martin, S. A. Jones and F. K. Akomeah, *Drug Delivery*, 2006, **13**, 175–187.
14 B. Zorec, V. Preat, D. Miklavcic and N. Pavselj, *Slov. Med. J.*, 2013, 339–356.
15 S. Rawat, S. Vengurlekar, B. Rakesh, S. Jain and G. Srikarti, *Indian J. Pharm. Sci.*, 2008, 3–10.
16 O. A. Hanbali, H. M. S. Khan, M. Sarfraz, M. Arafat, S. Ijaz and A. Hameed, *Acta Pharm.*, 2018, **69**, 197–215.
17 Y. H. An, J. Lee, D. U. Son, D. H. Kang, M. J. Park, K. W. Cho, S. Kim, S. H. Kim, J. Ko, M. H. Jang, J. Y. Lee, D. H. Kim and N. S. Hwang, *ACS Nano*, 2020, **14**, 4523–4535.
18 A. Ahsan, W. X. Tian, M. A. Farooq and D. H. Khan, *Int. J. Polym. Mater. Polym. Biomater.*, 2020, **8**, 574–584.
19 R. Parhi, *Adv. Pharm. Bull.*, 2017, **7**, 515–530.
20 C. J. Love, B. A. Serban, T. Katashima, K. Numata and M. A. Serban, *ACS Biomater. Sci. Eng.*, 2019, **5**, 5960–5967.
21 O. C. Onder, S. R. Batool and M. A. Nazeer, *Mater. Adv.*, 2022, **3**, 6920.
22 H. Zhang, D. Xu, Y. Zhang, M. Li and R. Chai, *Mater. Adv.*, 2022, **1**, e20220011.
23 H. H. Kim, D. W. Song, M. J. Kim, S. J. Ryu, I. C. Um, C. S. Ki and Y. K. Park, *Polymer*, 2016, **90**, 26–33.
24 N. Paradee and A. Sirivat, *J. Phys. Chem. B*, 2014, **118**, 9263–9271.
25 O. Bettucci, G. M. Matrone and F. Santoro, *Adv. Mater. Technol.*, 2021, 21002193.
26 P. M. Gotovtsev, G. U. Badranova, Y. V. Zubavichus, N. K. Chumakov, C. G. Antipova, R. A. Kamyshinsky, M. Y. Presniakov, K. V. Tokaev and T. E. Grigoriev, *Heliyon*, 2019, **5**, e02498.
27 A. P. Jou, E. Cazorla, G. Ruano, I. Babeli, M. P. Ginebra, J. G. Torres and C. Aleman, *ACS Biomater. Sci. Eng.*, 2020, **6**, 6228–6240.
28 X. Jin, C. Wei, C. Wu and W. Zhang, *ACS Omega*, 2022, **7**, 8493–8497.
29 A. Mahmood, A. Mahmood, R. M. Sarfraz, H. Ijaz, N. Zafar and M. U. Ashraf, *Polym. Bull.*, 2023, **80**, 8283–8319.
30 J. H. Ha, J. H. Lim, J. M. Lee and B. G. Chung, *Polymers*, 2023, **15**, 2608.
31 Y. Cai, J. Che, M. Yuan, X. Shi, W. Chen and W. Yuan, *Exp. Ther. Med.*, 2016, **12**, 2039–2044.
32 T. Saramas, P. Sakunpongpitiporn, K. Rotjanasuworapong, R. Morarad, S. Niamlang and A. Sirivat, *Int. J. Biol. Macromol.*, 2022, **223**, 702–712.
33 S. Mongkolkitikul, N. Paradee and A. Sirivat, *Eur. J. Pharm. Sci.*, 2018, **112**, 20–27.
34 N. Paradee, J. Thanokiang and A. Sirivat, *Mater. Sci. Eng., C*, 2020, **118**, 11346.
35 P. Sakunpongpitiporn, K. Phasuksom, N. Paradee and A. Sirivat, *RSC Adv.*, 2019, **9**, 6363.
36 D. Levasseur, I. Mjejri, T. Rolland and A. Rougier, *Polymers*, 2019, **11**, 179.
37 W. D. Loughneed, U. Fischer, K. Perlman and A. M. Albisser, *Diabetologia*, 1981, **20**, 51–53.
38 P. Sakunpongpitiporn, W. Naeowong and A. Sirivat, *Drug Delivery*, 2022, **29**, 2234–2244.
39 D. N. Rockwood, R. C. Preda, T. Yucel, X. Wang, M. L. Lovett and D. L. Kaplan, *Nat. Protoc.*, 2011, **6**, 1612–1631.
40 S. Yan, G. Han, Q. Wang, S. Zhang, R. You, Z. Luo, A. Xu, X. Li, M. Li, Q. Zhang and D. L. Kaplan, *Composites, Part B*, 2019, **176**, 107204.
41 T. Shen, T. Wang, G. Cheng, L. Huang, L. Chen and D. Wu, *Int. J. Biol. Macromol.*, 2018, **113**, 458–463.
42 M. H. Kim and W. H. Park, *Int. J. Nanomed.*, 2016, **11**, 2967–2978.
43 M. Correia, M. T. N. Petersen, P. B. Jeppesen, S. Gregersen and S. B. Petersen, *PLoS One*, 2012, **7**, e50733.
44 R. W. Korsmeyer, R. Gurny, E. Doelkar, P. Buri and N. A. Peppas, *Int. J. Pharm.*, 1982, **15**, 25–35.
45 T. Higuchi, *J. Pharm. Sci.*, 1961, **50**, 874–875.
46 D. Mikiewicz, A. B. Kryzsilk, A. Sobolewska, D. Stadnik, M. Bogiel, M. Pawlowska, A. W. Krawiec, P. A. Baran, N. Lukasiewicz, A. R. Chruscielewska, I. Sokolowska, J. Stadnik, P. Borowicz, G. Plucienniczak and A. Plucienniczak, *PLoS One*, 2017, 0172600.
47 K. Tari, S. Khamoshian, T. Madrakian, A. Afkhami, M. J. Los, A. Ghoorchian, M. R. Samarghandi and S. Ghavami, *Int. J. Mol. Sci.*, 2021, **22**, 12479.
48 J. J. Lee, S. Gandla, B. Lim, S. Kang, S. Kim, S. Lee and S. Kim, *NPG Asia Mater.*, 2020, **12**, 65.
49 H. Zheng and B. Zuo, *J. Mater. Chem. B*, 2020, **9**, 1238–1258.
50 N. Wu, H. Yu, M. Sun, Z. Li, F. Zhao, Y. Ao and H. Chen, *ACS Appl. Bio Mater.*, 2019, **3**, 721–734.
51 N. Johari, L. Moroni and A. Samadikuchaksaraei, *Eur. Polym. J.*, 2020, **134**, 109842.

52 M. Magos, J. Tapia and M. López, *Appl. Sci.*, 2020, **10**, 4995.
53 T. Vu, Y. Xue, T. Vuong, M. Erbe, C. Bennet, B. Palazzo, L. Popielski, N. Rodriguez and X. Hu, *Int. J. Mol. Sci.*, 2016, **17**, 1497.
54 H. Hong, O. J. Lee, Y. J. Lee, J. S. Lee, O. Ajiteru, H. Lee, Y. J. Suh, M. T. Sultan, S. H. Kim and C. H. Park, *Biomolecules*, 2020, **11**, 35.
55 A. Mikulska, J. Filipowska, A. M. Osyczka, M. Nowakowska and K. Szczubialka, *Front. Chem.*, 2015, **2**, 117.
56 D. T. Pham, N. Saelim and W. Tiyaboonchai, *J. Mater. Sci.*, 2018, **53**, 14087–14103.
57 R. H. Ansary, T. Roy and S. Easmin, *Am. J. Nano Res. Appl.*, 2020, **8**, 28–34.
58 Z. Chen, X. Zhang, J. Liang, Y. Ji, Y. Zhou and H. Fang, *Int. J. Mol. Sci.*, 2021, **22**, 7610.
59 A. Motta, C. Migliaresi, F. Faccioni, P. Torricelli, M. Fini and R. Giardino, *J. Biomater. Sci., Polym. Ed.*, 2004, **15**, 851–864.
60 M. Ribeiro, M. Moraes, M. Beppu, F. Monteiro and M. Ferraz, *Biomatter*, 2014, **4**, e28536.
61 Z. Du, C. Tang, Y. X. Guan, S. J. Yao and Z. Q. Zhu, *Int. J. Pharm.*, 2013, **454**, 174–182.
62 W. S. Chwedoruk, I. Malka, L. Bozycki, H. Nieznanska and W. Dzwolak, *PLoS One*, 2014, **9**, e86320.
63 U. H. Riversa, S. Kadian, S. Nejati, J. White, S. Sedaghat, Z. Mutlu and R. Rahimi, *ACS Sens.*, 2022, **7**, 960–971.
64 S. K. Mahatha and K. S. R. Menon, *J. Phys.: Condens.Matter*, 2012, **24**, 30552.
65 G. Kowalski, K. Kijowska, M. Witczak, L. Kuterasinski and M. Jukasiewicz, *Polymers*, 2019, **11**, 114.
66 H. W. Cho, H. B. Kim, J. Sung and J. S. Kim, *Polymers*, 2020, **12**, 2067.
67 J. Tavakoli, E. Jabbari, M. E. Khosroshahi and M. Boroujerdi, *Iran. Polym. J.*, 2006, **15**, 891–900.
68 S. Jin, J. Gu, Y. Shi, K. Shao, X. Yu and G. Yue, *Eur. Polym. J.*, 2013, **49**, 1871–1880.
69 A. Lammel, X. Hu, S. H. Park, D. L. Kaplan and T. Scheibel, *Biomaterials*, 2010, **31**, 4583–4591.
70 D. Fraser, T. Nguyen, A. Kotelsky, W. Lee, M. Buckley and D. S. W. Benoit, *ACS Biomater. Sci. Eng.*, 2022, **8**, 3568–3575.
71 R. Maeda, Y. Shinohara, H. Kawakami, Y. Isoda, I. Kanazawa and M. Mitsuishi, *Nanotechnology*, 2021, **32**, 135403.
72 G. Hoti, F. Caldera, C. Cecone, A. R. Pedrazzo, A. Anceschi, S. L. Appleton, Y. K. Monfered and F. Trotta, *Materials*, 2021, **14**, 478.
73 X. Zhao, Y. Zu, S. Zu, D. Wang, Y. Zhang and B. Zu, *Drug Dev. Ind. Pharm.*, 2010, **36**, 1177–1185.
74 K. Karthikeyan, S. Sekar, P. Devi, S. Inbaekaran, C. H. Lakshminarasaiah and T. P. Sastry, *J. Mater. Sci.: Mater. Med.*, 2011, **22**, 2721–2726.
75 L. Wang, C. Lu, B. Zhang, B. Zhao, F. Wu and S. Guan, *RSC Adv.*, 2014, **4**, 40312.
76 D. Kuang, F. Wu, Z. Yin, T. Zhu, T. Xing, S. C. Kundu and S. Lu, *Polymers*, 2018, **10**, 153.
77 Y. Zhang, M. Zhang, R. Zhang, H. Liu, H. Chen, X. Zhang, C. Li, Q. Zeng, Y. Chen and G. Huang, *Front. Mater.*, 2022, **9**, 914994.
78 R. S. Langer and N. A. Peppas, *Biomaterials*, 1981, **2**, 201–214.
79 M. Rizwan, R. Yahya, A. Hassan, M. Yar, A. D. Azzahari, V. Selvanathan, F. Sonsudin and C. N. Abouloula, *Polymers*, 2017, **9**, 137.
80 K. Ruangmak, N. Paradee, S. Niamlang, P. Sakunpongpitiporn and A. Sirivat, *J. Biomed. Mater. Res., Part B*, 2021, 1–11.
81 Z. W. Chaudryy, M. C. Gannon and F. Q. Nuttall, *Diabetes Care*, 2006, **29**, 493–497.
82 J. L. Knopp, L. H. Pearson and J. G. Chase, *J. Diabetes Sci. Technol.*, 2019, **13**, 597–600.
83 A. M. Chowdhury, R. I. Khan, S. S. R. NirzhorJabin, J. Jabin and A. I. Khan, *J. Innovations Pharm. Biol. Sci.*, 2017, **4**, 65–72.
84 O. Siddiqui, Y. Sun, J. C. Liu and Y. W. Chien, *J. Pharm. Sci.*, 1987, **76**, 341–345.
85 S. Kagatani, T. Shinoda, Y. Konno, M. Fukui, T. Ohmura and Y. Osada, *J. Pharm. Sci.*, 1997, **86**, 1273–1277.
86 K. Kajimoto, M. Yamamoto, M. Watanabe, K. Kigasawa, K. Kanamura, H. Harashima and K. Kogure, *Int. J. Pharm.*, 2010, **403**, 57–65.
87 Q. Pagneux, R. Ye, L. Chengnan, A. Barras, N. Hennuyer, B. Staels, D. Caina, J. I. A. Osses, A. Abderrahmani, V. Plasisance, V. Pawlowski, R. Boukherroub, S. Melinte and S. Szunerits, *Nanoscale Horiz.*, 2019, **5**, 663–670.